Planar intercalated Copper (II) complex molecule as small molecule enzyme mimic combined with Fe_3O_4 nanozyme for bienzyme synergistic catalysis applied to the microRNA biosensor

Liang Tian, Jinxu Qi, Olayinka Oderinde, Chen Yao, Wei Song, Yihong Wang

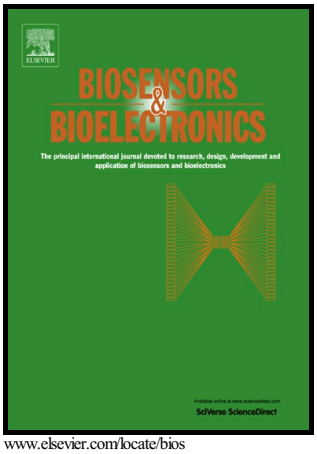

www.elsevier.com/locate/bios

PII: S0956-5663(18)30219-7
DOI: https://doi.org/10.1016/j.bios.2018.03.045
Reference: BIOS10371

To appear in: *Biosensors and Bioelectronic*

Received date: 6 January 2018
Revised date: 20 March 2018
Accepted date: 20 March 2018

Cite this article as: Liang Tian, Jinxu Qi, Olayinka Oderinde, Chen Yao, Wei Song and Yihong Wang, Planar intercalated Copper (II) complex molecule as small molecule enzyme mimic combined with Fe_3O_4 nanozyme for bienzyme synergistic catalysis applied to the microRNA biosensor, *Biosensors and Bioelectronic,* https://doi.org/10.1016/j.bios.2018.03.045

Planar intercalated Copper (II) complex molecule as small molecule enzyme mimic combined with Fe_3O_4 nanozyme for bienzyme synergistic catalysis applied to the microRNA biosensor

Liang Tian, Jinxu Qi, Olayinka Oderinde, Chen Yao, Wei Song, Yihong Wang*
School of Chemistry and Chemical Engineering, Southeast University, Nanjing, 211189, PR China.

Abstract

Enzyme mimics have been developed for bioassay of nucleic acids, with some of them involving complicated labeling. Herein, we report a label-free bioassay for ultrasensitive electronic determination of microRNA at an ultralow concentration based on target-triggered long-range self-assembly DNA-based hybridization chain reaction (HCR) protocol coupled with bienzyme mimics synergistic catalysis strategy. In this work, a planar intercalation molecule, copper (II) complex, is applied for the first time as a small molecule enzyme mimic as well as intercalation molecule in microRNA biosensor for signal amplification. Fe_3O_4 nanozyme were used as a separate and enriched target under magnetic field, and also in combination with HCR protocol detected in 3,3',5,5'-tetramethylbenzidine+hydrogen peroxide (TMB+H_2O_2) system to improve the sensitivity of the biosensor. Under optimal conditions, these strategies present good electrochemical behaviors for the detection of microRNA with a wide range from 100 aM to 100 nM and at relatively low detection limit of 33 aM. This remarkable sensitivity can make this proposed approach a promising scheme for development of next-generation microRNA sensors without the need of enzyme labeling or fluorophore labeling.

Graphical abstract

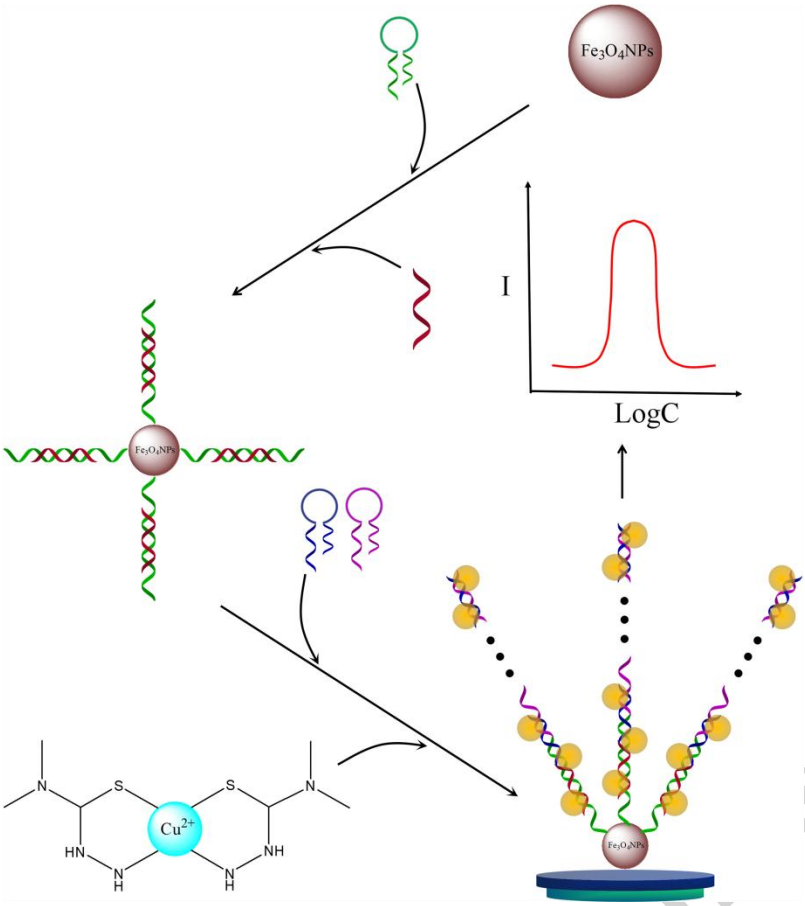

Keywords：Electrochemical biosensor; Hybridization chain reaction; Planar intercalated molecule; Copper (II) complex; Fe_3O_4 nanozyme; MicroRNA-21

1. Introduction

MicroRNAs are a kind of short, non-coding RNA molecules which possess an important regulatory effect in diverse biological processes in vivo, of whose abnormal expression may be related to the existence of cancer disease (Chen et al., 2018). Recently, microRNA-21 has been identified to be over-expressed in various cancers such as gastric-, esophagus-, prostate-, glioblastoma, neuroblastoma, breast- and lung cancers (Zhang et al., 2014). Hence, microRNAs detection has greatly attracted scientific interests for early clinical diagnosis of different diseases. However, the simple, precise, fast and low-cost quantification of microRNA is still a challenge. The most common methods for microRNA quantification are real-time fluorescent quantitative polymerase chain reaction (RT-PCR) (Markou et al., 2008), northern blotting (Marquez et al., 2010) and microarrays (Premaratne et al., 2017), which are found to be time-consuming and less sensitive. Electrochemical technique, on the other hand, has been considered as a promising

method for sensitive and selective microRNA detection due to its many advantages which include rapid, simple, sensitive, low-cost and easy high-throughput (Tian et al., 2018; Sekretaryova et al., 2016). Furthermore, the accurate, rapid, sensitive, selective detection for microRNAs by electrochemical technique requires a new type of signal amplification strategy (Gerasimova et al., 2014; Mandli et al., 2017).

Enzymes exhibit high biocatalytic activity and electron transfer reactivity, which are suitable as signal amplification molecules (Ye et al., 2014; Zhao et al., 2013). In enzyme signal amplification strategies, single enzyme catalysis (Zhang et al., 2012), bienzyme continuous catalysis and synergistic catalysis (Tian et al., 2015) have been reported. Most of the natural enzyme is composed of protein subunits, while some of them have essential RNA subunits (Houser-Scott et al., 2002); thus, inevitably suffer from some intrinsic drawbacks, such as expensive costs of extraction and separation, rigorous catalysis reaction condition, and weak stability due to protein denaturation (Gao et al., 2007), hence, the widespread application of these conventional natural enzymes is largely restricted. Nanozymes, a new type of mimic enzymes, have attracted much attention in recent years due to higher stability and lower cost (Wei et al., 2013). So far, various nanomaterials, such as gold nanoparticles (AuNPs) (Liu et al., 2017; Andoralov et al., 2013), Fe_3O_4 nanoparticles (Fu et al., 2017), CeO_2 nanoparticles (Liu et al., 2015), V_2O_5 nanowires (Huang et al., 2016) and Co_3O_4 nanoparticles (Golchin et al., 2017), have been discovered with oxidase (Chen et al., 2017), peroxidase (Li et al., 2018b), catalase (Hu et al., 2017), superoxide dismutase (Jiang et al., 2015), and laccase (Liang et al., 2017; Krikstolaityte rt al., 2014) mimicking activities. Fe_3O_4 nanoparticles, a superparamagnetic material, possesses peroxidase activity for signal amplification and could also be used to separate as well as enrich the target under external magnetic field.

In recent times, small molecule enzyme mimics such as metal-organic frameworks (MOFs) (Yang et al., 2017a) and metal complexes (Joshi et al., 2015) have gained much attention. Due to the several merits, which include acting as: (a) signal amplification molecules with enzyme-mimic catalytic activities; (b) intercalated molecules for RNA detection; and (c) a ligand of nanomaterials, the small molecule enzyme mimics have great potential to design new amplification strategy for label-free sensitive biosensor (Liu et al., 2016). In order to further improve the sensitivity for electrochemical detection of microRNA, many signal amplification strategies have been

developed, such as rolling circle amplification (RCA) (Lee et al., 2018), isothermal circular strand-displacement polymerization reaction (Giuffrida et al., 2015), nuclease-based target-recycling amplification (Li et al., 2016), and other enzyme mediated amplifications (Yang et al., 2017b) have been widely reported. However, these strategies usually require high cost of instrumentation and procurement of natural enzymes, as well as complex procedural steps, thereby limiting the practical application in clinic diagnosis of cancers. To avoid this inconvenience, the HCR strategy draws attractive attention. The HCR process is an isothermal alternative for DNA amplification without the involvement of any enzymes or thermal cycler (Yu et al., 2018). The rapidly emerging research field of HCR provides exciting possibilities for advanced development of new analytical tools.

Herein, we developed an electrochemical microRNA biosensor based on novel planar intercalation molecule copper (Cu) (II) complex coupled with target-triggered HCR strategy, as well as Cu(II) complex small molecule enzyme mimic with Fe_3O_4 nanozyme collaborative catalysis for signal amplification in the detection of microRNA-21. The hairpin capture probes (HCP) were immobilized onto the surface of Fe_3O_4 nanozyme, while the HCR reaction was carried out after binding with the target. DNA-based HCR driven by the free energy of the base pair formation without enzyme is a straightforward method for constructing one-dimensional DNA assemblies, created by the triggered self-assembly of two stable species of hairpin DNA 1 (HDNA1) and hairpin DNA 2 (HDNA2). The planar Cu(II) complex could intercalate well into the long-range DNA structures, while the Fe_3O_4 nanozyme was enriched on the surface of magnetic glassy carbon electrode (MGCE), which can be measured using electrochemical method, thereby resulting in the amplification of electrochemical signal. The signal amplification can further be achieved through the catalytic reaction of TMB+H_2O_2 system. Therefore, combining the above advanced aspects together, the proposed assay shows ultrahigh sensitivity and selectivity for target microRNA detection.

2. Experimental

2.1. Chemicals and reagents

4,4-dimethyl-3-thiosemicarbazide (ligand), tris-(2-carboxyethyl)-phosphine-hydrochloride

(TCEP) and 6-mercapto-1-hexanol (MCH) were purchased from Sigma-Aldrich, while N-(3-(dimethylaminopropyl)-N'-ethylcarbodiimide hydrochloride (EDC), N-hydroxysuccinimide (NHS), 30 % H_2O_2 and TMB were purchased from Aladdin Reagent Company (Shanghai, China). All other reagents used were of analytical grade. In our work, 10 mM phosphate buffered saline (PBS pH 6.0) was used as supporting electrolyte with pH adjustment being made with 0.1 M H_2SO_4 and 0.1 M NaOH. All aqueous solutions were prepared with ultrapure water (~18.2 MΩ·cm) using an Aquapro water purification system. The human serum samples of breast cancer patients and healthy individuals were supplied by the affiliated hospital of Qingdao University. Oligonucleotides were obtained from Sangon Biotech Co., Ltd (Shanghai, China). The sequences of these oligonucleotides were as follows: HCP: 5'-NH_3-TCAACATCAGTCTGATAAGCTACTACATGGACCGTTC-3'; target microRNA-21: 5'-UAGCUUAUCAGACUGAUGUUGA-3' (Chen et al., 2016); single-base mismatch microRNA: 5'-UAG CUU AUC GGA CUG AUG UUG A-3'; non-complementary microRNA: 5'-ACC GCA CAG GUG GAA UCU AAC G-3'; HDNA1: 5'-TCTAGCCACAACTCGGAACGGTCCATGTAG-3'; HDNA2: 5'-CGAGTTGTGGCTAGACTACATGGACCGTTC-3'.

2.2. Apparatus and measurements

The electrochemical measurements were carried out using the CHI 660E Electrochemical Workstation (Shanghai Chenhua Instrument Corporation, China) at room temperature. These include cyclic voltammetry (CV), electrochemical impedance spectroscopy (EIS) and differential pulse voltammetry (DPV). A conventional three electrode cell which consists of a modified 0.3 Tesla (T) MGCE (3 mm in diameter, working electrode), a platinum wire (auxiliary electrode) and a saturated calomel electrode (SCE, reference electrode) was used in all electrochemical investigations while EIS was performed in 5.0 mM $K_3Fe(CN)_6/K_4Fe(CN)_6$ mixture with 0.1 M KCl as supporting electrolyte, using an alternating current voltage of 5 mV, within the frequency range of 0.1-10^5 Hz. Transmission electron microscopy (TEM) images were obtained from a FEI Tecnai G2 T20 microscope (USA). While the magnetization measurements were carried out in an external field up by MGCE to 0.3 T at room temperature. A digital pH-meter (780 pH meter, Metrohm) was used to read the pH value of the buffer solutions. Electrolyte solutions were

deoxygenated by purging with pure nitrogen (99.99 %) for 10 min prior to electrochemical experiments. All measurements were carried out under a nitrogen atmosphere.

2.3. Synthesis of Fe_3O_4 NPs

The facile synthesis of citrate-coated Fe_3O_4 NPs was performed by following the procedure reported by Vallabani et al. (Vallabani et al., 2017) with slight modifications. Briefly, 1.8 gm $FeCl_3 \cdot 6H_2O$ and 0.9 gm $FeSO_4 \cdot 7H_2O$ salts were dissolved in 40 mL MilliQ water. At 80 °C, nitrogen gas was purged into the mixture, followed by the slow addition of 10 mL of NH_4OH (25 %), which made the solution turned black. The 80 °C temperature was maintained for further 30 min with continuous N_2 bubbling. Thereafter, using an external magnet, the NPs were pelleted down and the supernatant was discarded. The washing step was carried out for 4-5 times with boiled MilliQ water to remove excess ammonia. To the pellet solution (~15 mL), 1.25 gm of citric acid was added and stirred at 90 °C for 2 h. After cooling down to room temperature, Fe_3O_4 NPs were dialyzed for 24 h in MilliQ water using 12 KDa dialysis membrane (water was changed every 8 h). After dialysis, NPs were washed by centrifugation at 10,000 rpm for 10 min to remove the remnants. In the final step, the Fe_3O_4 NPs solution was centrifuged at 4000 rpm for 6 min and the supernatant was collected.

2.4. NH_3-HCP modification of Fe_3O_4 NPs

The activation of the modified magnetic beads was carried out in an EDC/sulfo NHS mixture solution (50 mg mL^{-1} each in MES buffer, pH 5.0) (Navarro et al., 2015). The blocking step was accomplished with a 1 M ethanolamine solution prepared in a 0.1 M phosphate buffer solution at pH 8.0, while the EDC was equilibrated to room temperature. Separately, 2 mg of Fe_3O_4 NPs was added to 200 µL conjugation buffer. A 2 mg of the NH_3-HCP dissolved in 500 µL of conjugation buffer was thereafter added to the already prepared 200 µL Fe_3O_4 NPs conjugation buffer. Another separate solution of 10 mg of EDC in 1 mL ultrapure water was prepared, of which 100 µL of this solution was immediately added into the mixed solution of Fe_3O_4 NPs and NH_3-HCP. The EDC-NH_3-HCP-Fe_3O_4NPs solution was then allowed to react for 12 hours at room temperature, followed by the purification of the conjugate using a centrifuge, after which it was then stored in a sterile container at 4 °C.

2.5. Synthesis of Cu(II) complex

Ligand (1 mmol) was dissolved in 10 mL methanol, followed by the addition of 0.5 mmol $Cu(NO_3)_2$ (dissolved in 15 mL methanol). The mixture was gently refluxed for 10 min. Upon cooling, the brown solution was volatilized slowly and single dark brown crystals of Cu(II) complex were obtained from the filtrate after few days. The Cu(II) complex was then isolated, washed three times with ethanol and dried in a vacuum desiccator, with the yield being 85 %. X-ray crystallographic data of Cu(II) complex were collected by a Bruker SMART Apex II CCD diffractometer using graphite-monochromated Mo-Ka (λ = 0.71073 Å) radiation while SADABS was used for empirical adsorption corrections. The structures were solved by Olex2 methods and refined against F^2 by full matrix least-squares methods using the Olex2 (Dolomanov et al., 2009). All of the atoms except H were refined anisotropically. Hydrogen atoms were placed in geometrically ideal positions and constrained to ride on their parent atoms by Olex2. The crystallographic data for Cu(II) complex are shown in Table S1. Finally, the Cu(II) complex was dissolved in an ultrapure water for further use.

2.6. Fabrication of target-triggered amplification biosensor

A MGCE was polished with 1.0, 0.3 and 0.05 μm aluminum slurry in turns and then sonicated in ethanol and ultrapure water for 1 min sequentially. The pretreated MGCE (diameter 3 mm) was immersed in a fresh piranha solution (98 % H_2SO_4 and 30 % H_2O_2, V/V 3:1) for about 30 min, followed by thorough rinsing with ultrapure water. 10 μL of a series of microRNAs samples were incubated with the 10 μL 86 mM Fe_3O_4/HCP at 37 °C for 1 h. Also, HDNA1 (5 μL 2 μM) and HDNA2 (5 μL 2 μM) were mixed for HCR at 37 °C for 2.5 h. Then, the Fe_3O_4/HCP/microRNAs/HDNA1/HDNA2 was magnetically decanted and incubated with 20 μL 4 μM Cu(II) complex to capture the signals at room temperature for 2 h. Thereafter, the Fe_3O_4/HCP/microRNAs/HDNA1/HDNA2/Cu(II) complex was decanted magnetically followed by redispersion in 20 μL pH 6.0 PBS. Finally, the above solution was dropped onto the cleaned MGCE, which have been blocked by 1 mM MCH for 1 h, while the Fe_3O_4/HCP/microRNAs/HDNA1/HDNA2/Cu(II) complex was fixed by MGCE under strong magnetic field of 0.3 T. After washing with water, DPV curves were collected in a potential range

of 0 V and +0.60 V with a pulse amplitude of 50 mV and a step potential of 4 mV in phosphate buffer saline (PBS, pH 6.0).

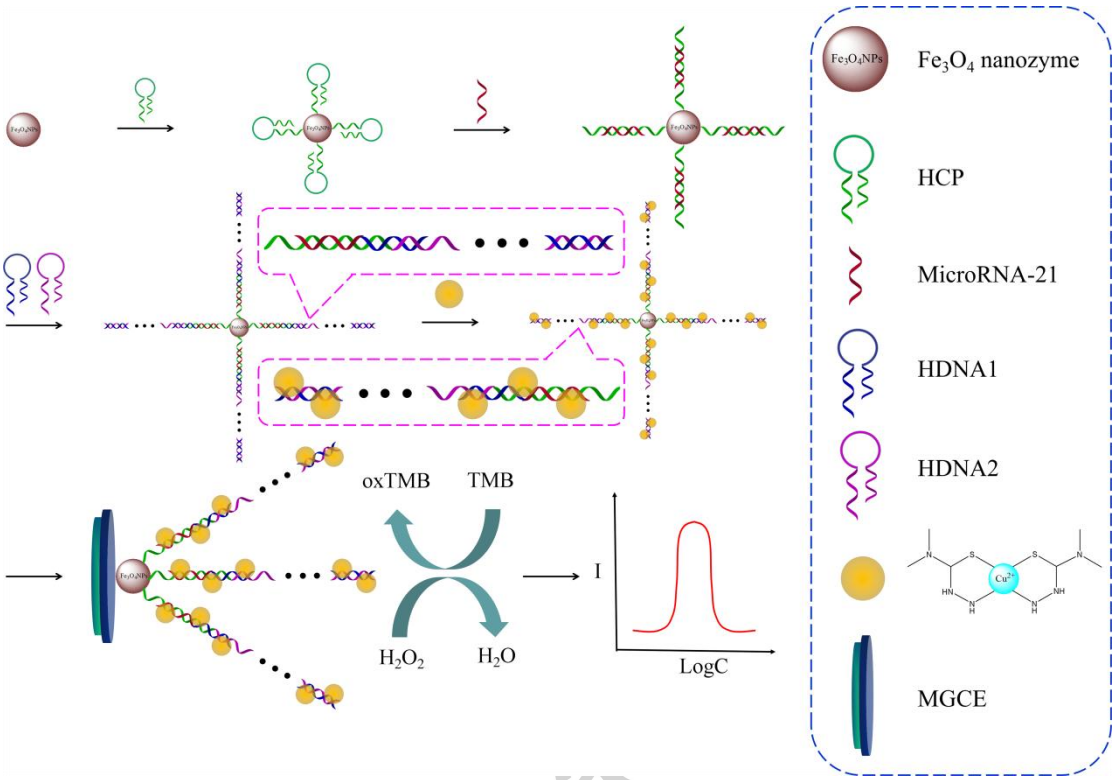

Scheme 1. Schematic representation of the microRNA biosensor and detection principle.

3. Result and discussion

3.1. Characterization of the magnetic nanoprobes

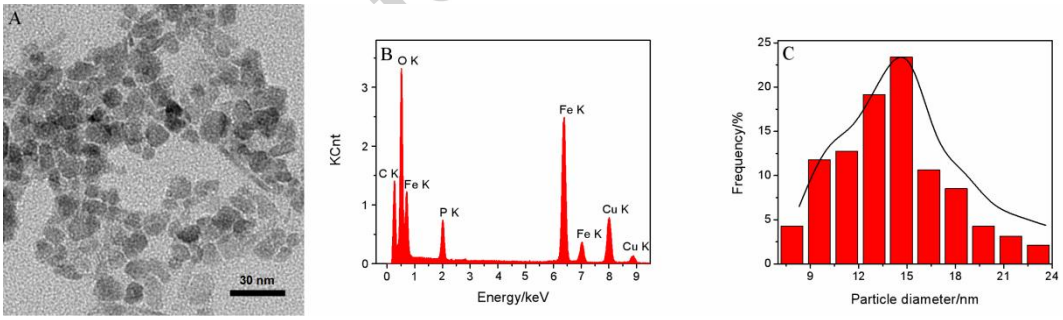

Fig. 1. Morphological and structural characterizations of HCP/Fe_3O_4NPs: TEM images (A), EDS analysis (B) and size distribution (C) of HCP/Fe_3O_4NPs.

In this work, HCP/Fe_3O_4NPs was prepared and used in the separation and enrichment of microRNA, as well as in the amplification of signal. The as-synthesized HCP/Fe_3O_4NPs were characterized by TEM as shown in Fig. 1A while the composition is displayed in EDS (Fig. 1B). The average particle diameter of the magnetic nanoprobes was around 14.5 nm (Fig. 1C). Such a

small size can reduce the steric hindrance of the space in addition to increasing the specific surface area, which indicated the advantage of excellent magnetic and easy separation properties of HCP/Fe_3O_4NPs.

3.2. Characterization of the Cu(II) complex

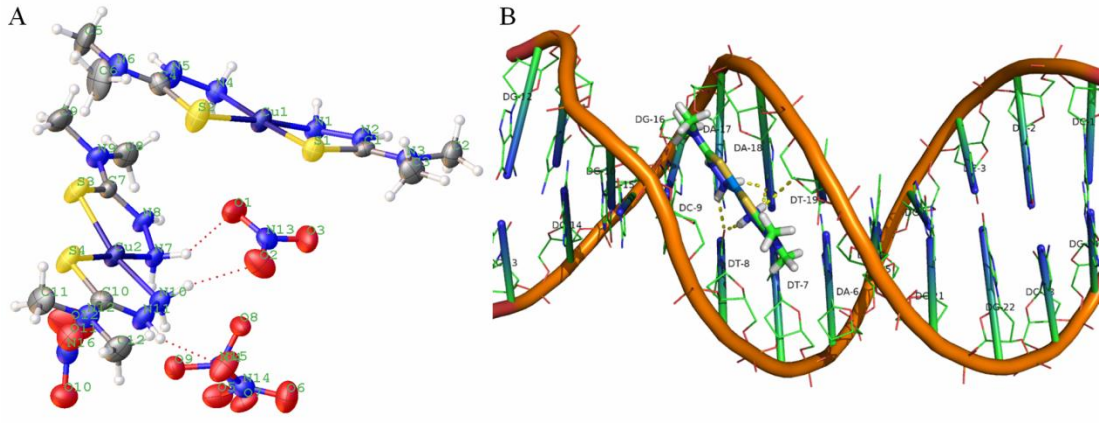

Fig. 2. (A) The molecular structures of Cu(II) complex showing the environment around the Cu(II) atom. Docking studies of Cu(II) complex and double stranded DNA using AutoDock: (B) the interaction mode between Cu(II) complex (showing stick representation) and double stranded DNA.

The 2:1 ligand/Cu(II) complex used in this work was successfully synthesized and determined by single-crystal X-ray diffraction. The complex was produced via the coordination of ligand with copper (II) nitrate. All of Cu(II) complex were crystallized out from the methanol solution with high purity without further purification. Taking the center of the copper, the sum of all the angles formed with the other four elements (N1, N4, S2, S1) equals 360 degrees. Furthermore, the Cu(II) complex was planar, with the molecular structures shown in Fig. 2A. The crystal data and structural refinement of Cu(II) complex were depicted in Table S1, while the bond angles and bond lengths were also shown in Table S2 and Table S3 respectively. And the mass spectrometry analysis has been applied to confirm the situation of the Cu(II) complex in solution as shown in Fig. S1. In order to express the intercalation binding of Cu(II) complex to double stranded DNA, the molecular docking simulation experiment was analyzed by AutoDock, with the binding of Cu(II) complex to double stranded DNA at the molecular level shown in Fig. 2B. The results showed that the planar Cu(II) complex could intercalate into the double stranded DNA skeleton via hydrogen bonds.

3.3. Principle of the electrochemical biosensor

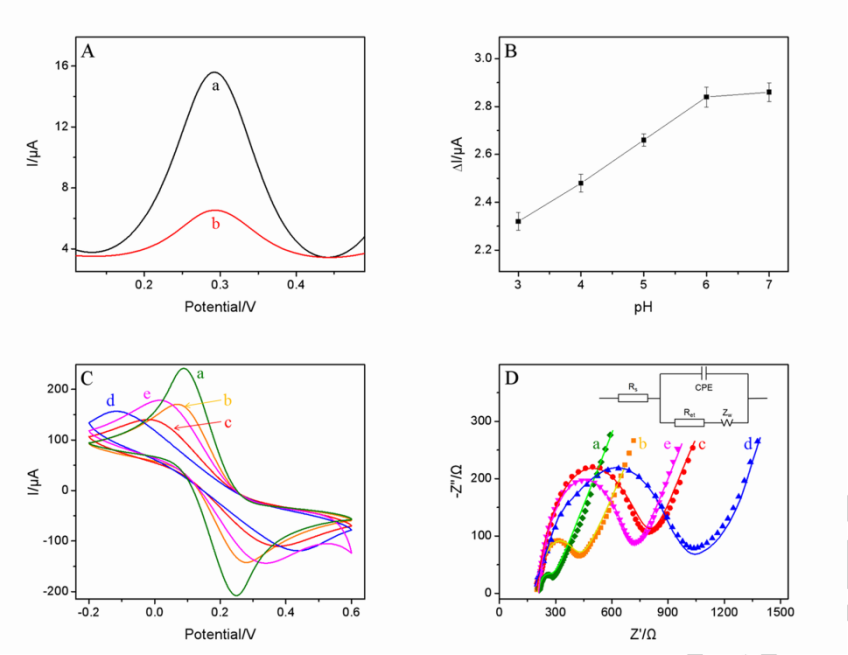

Fig. 3. DPV curves (A) of microRNA/HCP/Fe_3O_4NPs before (b) and after (a) HCR process in the presence of 100 pM microRNA-21 at the condition of 0.1 mM H_2O_2, 0.2 mM TMB and cultured with 4 μM Cu(II) complex obtained in 0.01 M PBS (pH=6.0). pH dependent peroxidase-like activity (B) of Cu(II) complex varied from 3 to 7 recorded by DPV in the presence of 1 μM Cu(II) complex, 0.1 mM H_2O_2 and 0.2 mM TMB. Error bars=RSD (n=5). CV (C) and EIS (D) of bare MGCE (a), Fe_3O_4/HCP (b), Fe_3O_4/HCP/microRNAs (c), Fe_3O_4/HCP/microRNAs/HDNA1/HDNA2 (d) and Fe_3O_4/HCP/microRNAs/HDNA1/HDNA2/Cu(II) complex (e) in 5.0 mmol L^{-1} $Fe(CN)_6^{4-/3-}$ containing 0.1 mol L^{-1} KCl at 100 mV s^{-1}. In addition, the frequency range is from 100 mHz to 100 kHz at 227 mV with amplitude of 5 mV (The inset is the equivalent circuit of the Nyquist plots).

In the presence of target microRNA, the HCP immobilized on the Fe_3O_4 nanozyme could open and hybridize the target, while the exposed part of HCP opens two alternating HDNA in turn, thereby propagate a chain reaction of hybridization events to form a nicked double-helix. Furthermore, numerous planar intercalation molecules of the Cu(II) complex were immobilized onto the long-range DNA nanostructures, each of which produces a strong electronic signal within the applied potentials. Fig. 3A exhibits the DPV response of HCP/Fe_3O_4NPs in the presence of target microRNA before and after HCR process to verify the validity of HCR after intercalation by Cu(II) complex. Compared with the blank (Fig. 3A, curve b), the reduction peak current of TMB at 0.29 V increased significantly after HCR in the presence of 100 pM microRNA-21 (Fig. 3A, curve a), which indicated that many Cu(II) complex have been captured by the microRNA-21 triggered HCR, while the Ipeak(a) was 12 μA, which is about four times higher than the Ipeak(b) of 3 μA. Thus, the HCR could remarkably increase the loading quantity of the signal molecules in

order to enhance signal amplification, while at the same time, the bienzyme mimic synergistic catalysis of Cu(II) complex and Fe_3O_4 nanozyme which is also used as magnetic carrier could improve the sensitivity of the biosensor, that could accurately detect microRNA-21 at lower concentration level. The reaction pH window of H_2O_2 catalysis was similar by using Fe_3O_4 NPs and Cu(II) complex, which have good synergistic catalysis as well as increased catalytic effect, hence Fe_3O_4 NPs and Cu(II) complex as synergistic catalysts were employed. Furthermore, a confirmation experiment of bienzyme mimic synergistic catalysis of Cu(II) complex and Fe_3O_4 nanozyme has been applied as shown in Fig. S2. In Fig. S2, the Ipeak of Cu(II) complex cultured with Fe_3O_4NPs/MGCE (5.25 μA) was higher than both Fe_3O_4NPs/MGCE (2.08 μA) and Cu(II) complex cultured with bare MGCE (1.41 μA), indicating that Cu(II) complex and Fe_3O_4 nanozyme have a good synergistic catalysis and increase the catalytic effect. The optimum pH window in TMB+H_2O_2 system of Fe_3O_4 NPs was around pH 6.0 according to the reference Navarro et al., 2015, while the optimum pH of Cu(II) complex was pH 6.0 as shown in Fig. 3B (Wu et al., 2009; Guo et al., 2015; Fang et al., 2014). ΔI was the Ipeak-$Ipeak_{(blank)}$ divided by $Ipeak_{(blank)}$, and the signal would get indpendent from the surface area of working electrode. The Fe_3O_4NPs and Cu(II) complex could catalyze the TMB by H_2O_2 to form TMB oxidation product, which could be reduced at the electrode surface to generate electrochemical reduction current. The peak potential of 0.29 V corresponds to the reduction of TMB.

3.4. Characterization of biosensor fabrication

In order to further verify the stepwise assembly processes of the modified electrodes, CV was employed. Fig. 3C illustrates typical CVs of $K_3[Fe(CN)_6]/K_4[Fe(CN)_6]$ at different surface electrodes, in which a couple of reversible redox peaks for the bare MGCE were observed (curve a). When HCP/Fe_3O_4NPs were immobilized onto the electrode, the peak current of the electrode decreases (curve b) due to the phosphates from the HCP could repulse ferri/ferrocyanide anions while the peak potential difference of redox peaks increases. Furthermore, after coating with the microRNA/HCP/Fe_3O_4NPs, the charge transfer ability of the microRNA/HCP/Fe_3O_4NPs became reduced, resulting in a decreased peak current response and a wider peak potential difference (curve c). These indicated that the adherence of microRNA effectively blocked the charge- and mass transfer between the redox couple in the solution and the MGCE electrode. Similarly, while

using HCR, the HDNA1/HDNA2/microRNA/HCP/Fe_3O_4NPs modified electrode resulted into a greater decrease in the peak current and a further increase in the peak potential difference (curve d). Following the addition of the Cu(II) complex into the modification, the redox of the $[Fe(CN)_6]^{3-/4-}$ ions on the modified electrode became more likely (curve e) as it exhibited a higher peak current response and a narrow peak potential difference. This means that the Cu(II) complex could improve the electron transport capability and reversibility of the biosensor after intercalation into the long range of DNA structure.

EIS is an effective tool for probing the features of surface-modified electrodes. The EIS measurements of the modified MGCE at different modification steps were carried out and the results in the form of Nyquist plot are illustrated in Figure 3D. The plot showed a semicircle in the high-frequency region and a straight line in the low frequency region, which demonstrated that the electrode process was being controlled by electron transfer at high frequency and by diffusion at low frequency. The spectra were analyzed by Zview2 software, which uses a nonlinear least-square fit to determine the parameters of the elements in the equivalent circuit, and consists of solution resistance (Rs), electron transfer resistance (Ret), constant-phase element (CPE), and Warburg impedance (Zw), as shown in the inset of Fig. 3D. It could be seen that the bare MGCE exhibited the smallest Ret value (curve a) while the HCP/Fe_3O_4NPs modified MGCE of 251 Ω (curve b) exhibited a higher Ret than the bare MGCE of 101 Ω (curve a). After the hybridization of HCP/Fe_3O_4NPs with microRNA, the MGCE surface generated an insulating layer on the electrode surface, which resulted in an obvious increase in Ret of 606 Ω (curve c). Subsequently, when the microRNA/HCP/Fe_3O_4NPs modified electrode was assembled with the HDNA1 and HDNA2 after HCR (curve d), the diameter of the semicircular part successively increased with the Ret also increasing to 934 Ω, suggesting that the electron transfer of the redox probe was obstructed by the assembled DNA strands, which invariably slowed down the redox reaction of $Fe(CN_6)^{3-/4-}$. However, the Ret value was decreased to 540 Ω when Cu(II) complex was further assembled into the HDNA1/HDNA2/microRNA/HCP/Fe_3O_4NPs electrode (curve e), which may be due to the ability of Cu(II) complex to facilitate electron-transfer. These results were consistent with the fact that the electrode was fabricated as expected and also well consistent with the phenomena in CVs, hence confirmed the successful preparation of the microRNA biosensor.

3.5. Optimization of experimental parameters

In order to optimize the condition for efficient detection, different parameters such as hybridization time and temperature were investigated. The effect of hybridization time on current signals of HDNA1/HDNA2/microRNA/HCP/Fe_3O_4NPs-modified electrode is shown in Fig. S3A. The microRNA/HCP/Fe_3O_4NPs was incubated in 5 µL of 2 µM HDNA1 and HDNA2 for HCR at 25 °C at varying incubation periods from 10 to 70 min. The results showed that the peak current increases rapidly with longer hybridization time from 10 to 60 min, reaching a saturation after 60 min. The saturated signal may be the result of complete hybridization of HDNA1 and HDNA2 with all available HCP anchored on the Fe_3O_4NPs. Based on this, considering sensitivity and assay time, the optimum hybridization time chosen was 60 min. Also, the effect of hybridization temperature was carried out by incubating microRNA/HCP/Fe_3O_4NPs with 5 µL of 2 µM HDNA1 and HDNA2 for 60 min at different temperatures ranging from 20 °C to 40 °C, with the results showing that as hybridization temperature increases from 20 °C to 30 °C, the peak current value also increases, depicting a higher amount of hybridized HDNA1 and HDNA2 by the HCP. However, a further increase in hybridization temperature above 30 °C resulted in the decrease of peak current value (Fig. S3B). This could be due to the effect of temperature on the thermodynamic properties for DNA duplex formation, thereby affecting the hybridization efficiency between DNA strand and HCP (Wu et al., 2002). Consequently, the optimized hybridization temperature adopted for the biosensor was 30 °C.

3.6. Electrochemical Determination of microRNA-21 by DPV

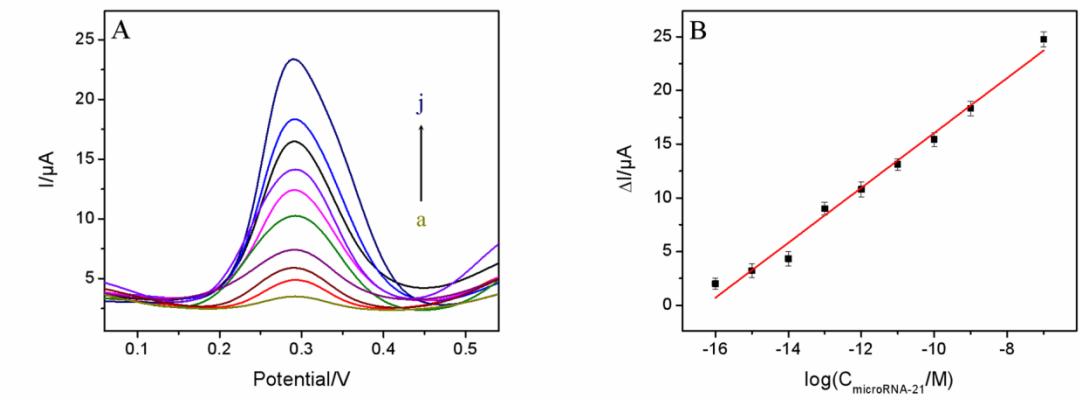

Fig. 4. DPV responses (A) to MGCE/Fe_3O_4/HCP/microRNAs/HDNA1/HDNA2/Cu(II) complex fabricated

biosensor after capturing different concentrations of microRNA-21 from (a) to (j): 0 M, 100 aM, 1 fM, 10 fM, 100 fM, 1 pM, 10 pM, 100 pM, 1 nM and 100 nM in 0.01 M PBS (pH=6.0) with 0.1 mM of H_2O_2 and 0.2 mM of TMB. (B) Calibration curve of net peak current vs. logarithmic microRNA-21 concentration. Error bars=RSD (n=5).

The sensitivity of the assay was studied under the optimized conditions, and the target microRNA-21 quantified with the established magnetic electrochemical sensing system. Fig. 4A showed the corresponding DPV curves towards different concentration of microRNA-21. The reduction peak current values increase with the increase in concentration of microRNA-21 from zero to 100 nM (Fig. 4A). A wide detection range between 100 aM and 100 nM (R^2=0.9851) was obtained, with the equation being $\Delta I = 41.64+2.56\log(C_{microRNA\text{-}21}/M)$ as shown in Fig. 4B , $\Delta I = (Ipeak_{(microRNA)}\text{-}Ipeak_{(blank)})/Ipeak_{(blank)}$, and at a detection limit of 33 aM (S/N=3), indicating that the detection limit of our magnetic electrochemical microRNA-21 sensing system is more enhanced when compared with other methods as shown in Table 1. Compared to traditional protocols, the bienzyme mimic signal amplification strategy combined with HCR protocol exhibited a higher sensitivity and wide detection range. Along with the advantages of its rapidity, simplicity and precision, the magnetic electrochemical microRNA sensing system is of great importance for the application in detecting microRNA in real samples.

3.7. Specificity and reproducibility of the biosensor

The selectivity of the sensor was investigated by mismatch target microRNAs. To verify this, single base mismatch target microRNA and non-complementary target microRNA for the selectivity analysis were used. The concentration of all microRNA sequences used in the selectivity evaluation was 100 pM. A comparison of the sensing performance with complementary microRNA, single base mismatch target microRNA and non-complementary target microRNA are shown in Fig. S4A. The peak current value response for single base mismatch sequences and non-complementary sequences was ~21 % and ~9 % respectively. The high sequence selectivity may be attributed to the unique and essential selectivity of the term hairpin capture probe. The result showed that the sensor is selective to the microRNA sequences and can be used to detect mismatch sequences even to the level of single base mismatch, as well as further differentiate any mismatch microRNA sequences from the target microRNA.

To test the reproducibility of the microRNA biosensor, six working electrodes were treated

under the same conditions to detect the target microRNA (100 pM). The results are shown in Fig. S4B with the relative standard deviation (RSD) being 3.8 % (n=5), which indicates the excellent reproducibility of designed biosensor.

3.8. Detection of target microRNA in real samples

To demonstrate the real applicability of this proposed approach on the assay of microRNA-21 in real serum samples, the human serum samples from 5 breast cancer patients and 5 healthy donors were evaluated. As shown in Fig. S5, the the breast cancer patients serum generated an increasing DPV signal (7.103 μA) about 3 times higher than that obtained from the healthy donors serum (2.374 μA), $\Delta I = (Ipeak\text{-}Ipeak_{(blank)})/Ipeak_{(blank)}$, suggesting an up-regulation of miRNA-21 expression in the breast cancer human serum. This result is in good agreement with reported literatures (Hong et al., 2013), and this ultrasensitive electrochemical microRNA biosensor has a promising future in the area of microRNA diagnostics and clinical analysis.

4. Conclusion

An ultrasensitive electrochemical biosensor was fabricated for the detection of microRNA on the basis of HCR reaction for highly efficient bienzyme mimic cascade amplification. Herein, Cu(II) complex were employed as both the planar intercalation molecule and signal amplification molecule with Fe_3O_4 nanozyme to catalyze the reduction of H_2O_2 in order to generate ·OH for the oxidation of TMB. In addition, the Fe_3O_4 nanozyme could be used for the separation and enrichment of the target under magnetic field, as well as for the signal amplification molecule, leading to enhanced immobilization efficiency of the target with higher catalytic efficiency. The MGCE increases the accessibility and reactivity, as well as prevents the decrease of signal molecules in the construction process of the biosensor. The microRNA induced hairpin opening and the subsequent HCR assisted the localization of Cu(II) complex. After the dual signal amplification, the reduction peak of TMB is recorded to represent microRNA levels. Also, the sensitivity of this microRNA biosensor significantly improves. A linear range from 100 aM to 100 nM and detection limit of 33 aM were also achieved. The proposed method does not only exhibit excellent analytical characteristics, but also has other advantages such as easy operation,

nonenzymatic detection and fine reproducibility, which ensures its great potential for biological research and clinical diagnostics.

Acknowledgements

This research was financially supported by the National Nature Science Foundations of China (No. 81571812) and A Project Funded by the Priority Academic Program Development of Jiangsu Higher Education Institutions (1107047002).

References

Andoralov, V., Shleev, S., Arnebrant, T., Ruzgas, T., 2013. Anal. Bioanal. Chem. 405, 3871-3879.

Chen, A.Y., Ma, S.Y., Zhou, Y., Chai, Y.Q., Yuan, R., 2016. Anal. Chem. 88, 3203-3210.

Chen, S., Quan, Y., Yu, Y.L., Wang, J.H., 2017. ACS Biomater. Sci. Eng. 3, 313-321.

Chen, Y.X., Huang, K.J., Niu, K.X., 2018. Biosens. Bioelectron. 99, 612-624.

Diao, W., Tang, M., Ding, S.J., Li, X.M., Cheng, W.B., Mo, F., Yan, X.Y., Ma, H.M., Yan, Y.R., 2018. Biosens. Bioelectron. 100, 228-234.

Dolomanov, O.V., Bourhis, L.J., Gildea, R.J., Howard, J.A.K., Puschmann, H., 2009. J. Appl. Cryst. 42, 339-341.

Fan, X.J., Qi, Y., Shi, Z.Y., Lv, Y.K., Guo, Y.J., 2018. Sensor. Actuat. B-Chem. 255, 1582-1586.

Fang, X., Bai, L.J., Han, X.W., Wang, J., Shi, A.Q., Zhang, Y.Z., 2014. Anal. Biochem. 460, 47-53.

Fu, S.Y., Wang, S., Zhang, X.D., Qi, A.H., Liu, Z.R., Yu, X., Chen, C.F., Li, L.L., 2017. Colloid. Surface. B. 154, 239-245.

Gao, L.Z., Zhuang, J., Nie, L., Zhang, J.B., Zhang, Y., Gu, N., Wang, T.H., Feng, J., Yang, D.L., Perrett, S., Yan, X.Y., 2007. Nat. Nanotechnol. 2, 577-583.

Gerasimova, Y.V., Kolpashchikov, D.M., 2014. Chem. Soc. Rev. 43, 6405-6438.

Giuffrida, M.C., Zanoli, L.M., D'Agata, R., Finotti, A., Gambari, R., Spoto, G., 2015. Anal. Bioanal. Chem. 407, 1533-1543.

Golchin, J., Golchin, K., Alidadian, N., Ghaderi, S., Eslamkhah, S., Eslamkhah, M., Akbarzadeh, A., 2017. Artif. Cell. Nanomed. B. 45, 1069-1076.

Guo, J.J., Han, X.W., Wang, J.C., Zhao, J.Q., Guo, Z.L., Zhang, Y.Z., 2015. Anal. Biochem. 491,

58-64.

Hong, C.Y., Chen, X., Liu, T., Li, J., Yang, H.H., Chen, J.H., Chen, G.N., 2013. Biosens. Bioelectron. 50, 132-136.

Houser-Scott, F., Xiao, S.H., Millikin, C.E., Zengel, J.M., Lindahl, L., Engelke, D.R., 2002. P. Natl. Acad. Sci. USA 99, 2684-2689.

Hu, M.H., Korschelt, K., Daniel, P., Landfester, K., Tremel, W., Bannwarth, M.B., 2017. ACS Appl. Mater. Inter. 9, 38024-38031.

Huang, Y.Y., Liu, Z., Liu, C.Q., Ju, E.G., Zhang, Y., Ren, J.S., Qu, X.G., 2016. Angew. Chem. Int. Edit. 55, 6646-6650.

Jiang, Y.H., Brynskikh, A.M., S-Manickam, D., Kabanov, A.V., 2015. J. Control. Release 213, 36-44.

Joshi, T., Graham, B., Spiccia, L., 2015. Acc. Chem. Res. 48, 2366-2379.

Krikstolaityte, V., Barrantes, A., Ramanavicius, A., Arnebrant, T., Shleev, S., Ruzgas, T., 2014. Bioelectrochemistry 95, 1-6.

Lee, C.Y., Fan, H.T., Hsieh, Y.Z., 2018. Sensor. Actuat. B-Chem. 255, 341-347.

Li, B.C., Yin, H.S., Zhou, Y.L., Wang, M.H., Wang, J., Ai, S.Y., 2018a. Sensor. Actuat. B-Chem. 255, 1744-1752.

Li, C.X., Wang, H.Y., Shen, J., Tang, B., 2015. Anal. Chem. 87, 4283-4291.

Li, J., Cao, Y., Hinman, S.S., McKeating, K.S., Guan, Y.W., Hu, X.Y., Cheng, Q., Yang, Z.J., 2018b. Biosens. Bioelectron. 100, 304-311.

Li, Y.C., Zhang, J.Y., Zhao, J.J., Zhao, L.K., Cheng, Y.Q., Li, Z.P., 2016. Analyst 141, 1071-1076.

Liang, H., Lin, F.F., Zhang, Z.J., Liu, B.W., Jiang, S.H., Yuan, Q.P., Liu, J.W., 2017. ACS Appl. Mater. Inter. 9, 1352-1360.

Liu, B.W., Sun, Z.Y., Huang, P.J.J., Liu, J.W., 2015. J. Am. Chem. Soc. 137, 1290-1295.

Liu, L., Shi, Y., Yang, Y.F., Li, M.L., Long, Y.J., Huang, Y.M., Zheng, H.Z., 2016. Chem. Commun. 52, 13912-13915.

Liu, Y., Ding, D., Zhen, Y.L., Guo, R., 2017. Biosens. Bioelectron. 92, 140-146.

Mandli, J., Mohammadi, H., Amine, A., 2017. Bioelectrochemistry 116, 17-23.

Markou, A., Tsaroucha, E.G., Kaklamanis, L., Fotinou, M., Georgoulias, V., Lianidou, E.S., 2008. Clin. Chem. 54, 1696-1704.

Marquez, R.T., Wendlandt, E., Galle, C.S., Keck, K., MacCaffrey, A.P., 2010. Am. J. Physiol-Gastr. L. 298, G535-G541.

Miao, P., Tang, Y.G., Yin, J., 2015. Chem. Commun. 51, 15629-15632.

Navarro, J.R.G., Conzatti, G., Yu, Y., Fall, A.B., Mathew, R., Eden, M., Bergstrom, L., 2015. Biomacromolecules 16, 1293-1300.

Premaratne, G., Mubarak, Z.H.A., Senavirathna, L., Liu, L., Krishnan, S., 2017. Sensor. Actuat. B-Chem. 253, 368-375.

Sekretaryova, A.N., Eriksson, M., Turner, A.P.F., 2016. Biotechnol. Adv. 34, 177-197.

Shuai, H.L., Wu, X., Huang, K.J., Zhai, Z.B., 2017. Biosens. Bioelectron. 94, 616-625.

Tian, J.Y., Huang, T., Wang, P., Lu, J.S., 2015. J. Electrochem. Soc. 162, B319-B325.

Tian, L., Qian, K., Qi, J.X., Liu, Q.Y., Yao, C., Song, W., Wang, Y.H., 2018. Biosens. Bioelectron. 99, 564-570.

Vallabani, N.V.S., Karakoti, A.S., Singh, S., 2017. Colloid. Surface. B. 153, 52-60.

Wei, H., Wang, E.K., 2013. Chem. Soc. Rev. 42, 6060-6093.

Wei, T.X., Du, D., Wang, Z.Y., Zhang, W.W., Lin, Y.H., Dai, Z.H., 2017. Biosens. Bioelectron. 94, 56-62.

Wu, P., Nakano, S.I., Sugimoto, N., 2002. Eur. J. Biochem. 269, 2821-2830.

Wu, Y., Zheng, J.W., Li, Z., Zhao, Y.R., Zhang, Y., 2009. Biosens. Bioelectron. 24, 1389-1393.

Xiong, E.H., Li, Z.Z., Zhang, X.H., Zhou, J.W., Yan, X.X., Liu, Y.Q., Chen, J.H., 2017. Anal. Chem. 89, 8830-8835.

Yang, H.G., Yang, R.T., Zhang, P., Qin, Y.M., Chen, T., Ye, F.G., 2017a. Microchim. Acta 184, 4629-4635.

Yang, X., Lv, J.J., Yang, Z.H., Yuan, R., Chai, Y.Q., 2017b. Anal. Chem. 89, 11636-11640.

Ye, S.J., Mao, Y.N., Guo Y.Y., Zhang, S.S., 2014. TrAC-Trend. Anal. Chem. 55, 43-54.

Yuan, Y.H., Wu, Y.D., Chi, B.Z., Wen, S.H., Liang, R.P., Qiu, J.D., 2017. Biosens. Bioelectron. 97, 325-331.

Yu, B., Li, F.L., Zhao, T.C., Li, F., Zhou, B.Q., Xu, H.Y., 2018. Sensor. Actuat. B-Chem. 256, 624-631.

Zhang, K., Dong, H.F., Dai, W.H., Meng, X.D., Lu, H.T., Wu, T.T., Zhang, X.J., 2017. Anal. Chem. 89, 648-655.

Zhang, M.N., Yu, P., Mao, L.Q., 2012. Acc. Chem. Res. 45, 533-543.

Zhang, Y., Yang, P.Y., Wang, X.F., 2014. Trends Cell Biol. 24, 153-160.

Zhao, J., Yan, Y.L., Zhu, L., Li, X.X., Li, G.X., 2013. Biosens. Bioelectron. 41, 815-819.

Zhuang, J.Y., Han, B., Liu, W.C., Zhou, J.F., Liu, K.W., Yang, D.P., Tang, D.P., 2018. Biosens. Bioelectron. 99, 230-236.

Table 1 Comparison of different biosensors for determination of nucleic acids.

Method	Analyte	Method of signal amplification	Linear arrange	Detection limit	Reference
Electrochemical Ratiometric Biosensor	DNA	AuE/MB-DNA/MCH /Fc-DNA/target DNA	0.5 pM-80 pM	0.12 pM	(Xiong et al., 2017)
Photoelectrochemical	Let-7a microRNA	Gold disk/hairpin probe/target microRNA/ALP-Ls	0.1 pM-1 nM	0.075 pM	(Zhuang et al., 2018)
Surface Plasmon Resonance	DNA	Gold sensing chip/hairpin capture probes/HIV-related DNA ESDRs/DDTs	1 pM-150 nM	48 fM	(Diao et al., 2018)
Fluorescence	microRNA-21	AuNPs-MBs/dithiol-anti-microRNA/microRNA/DTDI-AlbNPs-p19 protein	10 fM-10 nM	9 fM	(Wei et al., 2017)
Photoelectrochemical Biosensor	DNA	ITO/Cp-DNA/MCH/target DNA/H1&H2(HCR)/Ir(III) complex	0.025 pM-100 pM	9 fM	(Li et al., 2015)
Fluorescence	Let-7a	GO/H1&H2/RecQE	10 fM-2 pM	4.2 fM	(Fan et al.,

	microRNA	&ATP/target microRNA (HCR)			2018)
Amperometric /DPV	microRNA-21	AuE/hairpin capture probe/MCH/microRNA-21/SA-Pt-Sn-In_2O_3	0.5 fM-5 pM	1.92 fM	(Zhang et al., 2017)
Photoelectrochemical	microRNA-319a	ITO/CuO-$CuWO_4$/Au/AuNPs/ssDNA/Target RNA (RCA)/Phos-tag-biotin/avidin-ALP	1 fM-0.1 nM	0.47 fM	(Li et al., 2018a)
Amperometric /DPV	microRNA-141& microRNA-21	AuE/HCP1&HCP2/MCH/microRNA-141 & microRNA-21/HDNA1@HDNA1' & HDNA2@HDNA2'(HCR)/DNA1@Fe_3O_4NPs@Thi & DNA2@Fe_3O_4NPs@Fc	1 fM-1 nM	0.44 fM (microRNA-141)& 0.46 fM (microRNA-21)	(Yuan et al., 2017)
Amperometric /DPV	DNA	GCE/SiO_2@$MoSe_2$-AuNPs/capture probe/MCH/DNA linked GO-AuNPs hybrids/Target DNA/Bio-H1&Bio-H2(HCR)/Avidin-HRP	0.1 fM-100 pM	0.068 fM	(Shuai et al., 2017)
Amperometric /LSV	Hsa-microRNA-17-5p	AuE/Tetrahedral DNA with hairpin capture probe/microRNA/HCR-H0 modified AuNPs/HCR-H1-AgNPs/HCR-H2-AgNPs	100 aM-100 pM	2 aM	(Miao et al., 2015)
Amperometric /DPV	microRNA-21	MGCE/Fe_3O_4 nanozyme-hairpin capture probe/microRNA/HDNA1&HDNA2(HCR)/Cu(II) complex	100 aM-100 nM	33 aM	This work

Highlights

- An original planar intercalation molecule was developed for electrochemical microRNA detection.
- Magnetic field induced targeted separation and enrichment coupled with hybridization chain reaction.
- Fe_3O_4 nanozyme with copper (II) complex bienzyme mimic synergistic catalysis for signal amplification.
- An ultralow detection limit of 33 aM was obtained with good selectivity and repeatability.